Volume 1 | Number 1 | Jan 2013 | Pages 1–100

Journal of
Materials Chemistry A

Materials for energy and sustainability
www.rsc.org/materialsA

ROYAL SOCIETY
OF CHEMISTRY

ROYAL SOCIETY
OF CHEMISTRY

www.rsc.org/materialsA

Journal Name

ARTICLE

Anatase TiO₂ Nanocubes for Fast and Durable Sodium Ion Battery Anodes

Xuming Yang,[a] Chao Wang,[b] Yingchang Yang,[a] Yan Zhang,[a] Xinnan Jia,[a] Jun Chen,[a] Xiaobo Ji*[a]

Aimed at an advanced anatase TiO₂ anode for sodium ion batteries, crystalline titania nanocubes were employed and delivered a gradually increasing capacity at initial cycles termed as an activation process. The necessary discharge-charge loops for total activation is dependent on galvanostatic current density (about 20 cycles at 0.2C while 90 cycles at 1C). A percentage of Ti^{3+} was detected after the activation, indicating an amount of irreversibly trapped sodium ions in the lattice. After the activation process excellent rate capability and outstanding cycle stability were presented. The reversible capacity reached 174, 132, and 108 mAh g⁻¹ at the rate of 1C, 5C, and 10C. And the capacity was well sustained with a loss less than 10% within 1000 discharge-charge cycles at the rate of 2C or 10C. The superior battery performance achieved by the nanocubes is supposed to be related to the encircled {100 facets that is more favorable for sodium ion attachment than {001} and {101} facets supported by first-principles calculations. And from this work we see the feasibility of optimizing electrode materials via rational surface structure construction based on theoretic calculations.

1. Introduction

Lithium ion batteries (LIBs) have taken a dominant market position as power sources for portable electronic devices, and hold a rapidly increasing share in the battery supply for hybrid or pure electric vehicles.[2-4] As sodium ions owns only a slight larger size than lithium ions and exhibit similar chemistry, the success achieved in LIBs is promising to be repeated in the sodium ion batteries (NIBs).[5-8] The sodium-ion system is even more competitive in large-scale stationary applications, in terms of material cost, as sodium is readily available from crust and sea water, while lithium resource has relatively quite a limited abundance and a severely inhomogeneous distribution in the Earth.[5] It also holds advantages in the respect of electrolyte due to the high ion conductivity of sodium ion based electrolyte[11] and the low desolvation energy of sodium ions in polar solvents[13]. Presently, the gravimetric capacity of electrode materials for NIBs has been comparable to that for state-of-the-art LIBs, and the battery performance has been significantly improved though not yet enough for commercialization.[6, 14] Not surprisingly, researches on NIB electrode materials are drawing more and more scientific enthusiasm.

Titanium-based compounds such as titanium dioxide (TiO₂) and sodium titanate (Na₂Ti₃O₇) are regarded as promising candidates for NIB anodes because of their low sodiation/desodiation voltage, natural abundance and environmental benign.[1, 9, 15-17] Relevant research is targeted to improving its electrochemical performance, mainly in the aspects of rate capability and durability that are their most attractive vantages in Li-ion system[16, 18], by nanostructure constructions,[19] electrolyte optimization[10] and so on. The excellent rate capability is highly emphasized since the capacity of titanium-based anodes is much lower than hard carbon[20], tin or antimony-based materials[21, 22], et al. On another hand the feasibility of long-term operation is a key consideration, especially when utilized in stationary energy storage systems where NIBs would probably be positioned in the market.[7]

Aiming at advancing anatase TiO₂ anodes, we managed to prepare anatase TiO₂ nanocubes enclosed by {100} and {001} facets[23] and systematically explored its electrochemical property as NIB anodes. Compared with previous reported works,[1, 9, 10, 12] it showed an excellent rate capability and cycle stability after a gradual activation process. And first-principles investigation were conducted to help comprehend such a superiority.

2. Results and discussion

2.1 Structure characterization
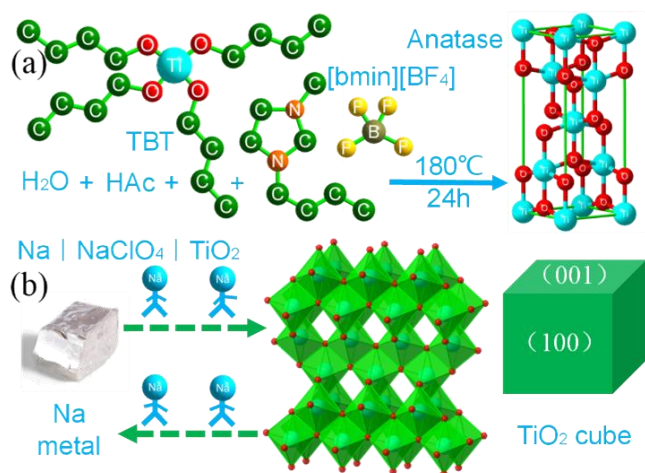
Figure 1. Schematics of the synthesis routine (a) and the configuration of half sodium ion batteries (b).

Herein the anatase TiO_2 nanocubes were obtained from the hydrolysis of tetrabutyl titanate (TBT) in a mixed composition of water (H_2O), acetic acid (HAc) and ionic liquid 1-butyl-3-methylimidazolium tetrafluoroborate ([bmin][BF_4]) under hydrothermal conditions at 180 ℃ for 24 hours, as schematically displayed in Figure 1a. Such a quaternary solution system is derived from a reported work where titanate tetra-isopropoxide (TTIP) was used and the anatase TiO_2 output is only about 50 mg.[23, 24] In order to scale the preparation with a cubic or near-cubic shape, we had the molar ration of H_2O, [bmin][BF_4], and HAC to be 41.5:2:210, chosen TBT that owns a slower hydrolysis speed instead of TTIP as the titanate source and increased the input up to be five times. To put it simply, 5 mL of TBT, 2.5 mL of H_2O, 1 mL of [bmin][BF_4], and 40 mL of HAc were blended and formed a homogeneous quaternary solution before hydrothermal processing. The resultant product weight about 1.2 g after being rinsed and dried.

The sample turned out to be well-shaped nanocubes as presented in the SEM (scanning electron microscope, Figure 2a) image. It had a uniform size distribution and was almost mono-dispersed. In the transmission electron microscope (TEM, Figure 2b) image, the edge length is measured to be 80~100 nm that is well consistent to the SEM result. These nanocubes were characterized to be pure anatase type via the X-ray diffraction
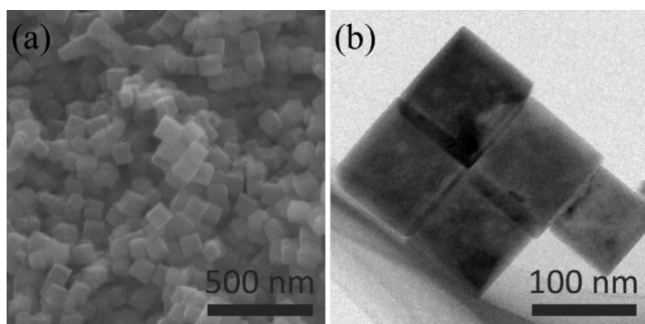
Figure 2. The SEM and TEM images of anatase TiO_2 nanocubes.
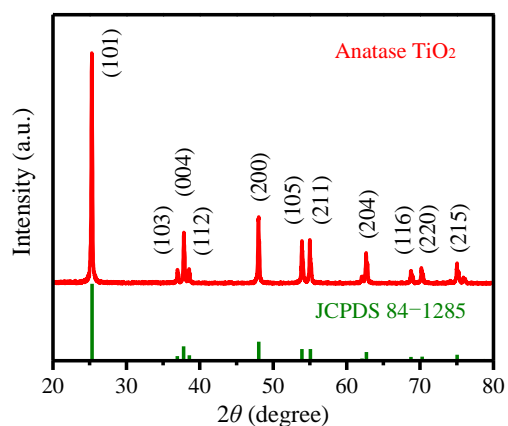
Figure 3. The XRD pattern of anatase TiO_2 nanocubes.

pattern (XRD, Figure 3). All the peaks are perfectly indexed to JCPDS No.84-1285 (space group $I4_1/amd$, a=3.785 Å, c=9.512 Å), and they are extremely sharp that manifests a high crystallization.

2.2 Electrochemical activation process

The battery performance was evaluated from a configured half sodium cell with metallic sodium served as reference and count electrode (Figure 1b). It delivered a gradually increasing capacity as in the precedents of amorphous TiO_2 nanotubes and anatase TiO_2 nanoparticles (Figure 4).[1, 10] At the galvanostatic current of 0.2C (Figure 4a, 1C was defined to be 168 mA g^{-1} as in the lithium-ion system), the discharge and charge capacity was measured to be 192 and 73 mAh g^{-1} in the first cycles, thus the initial coulombic efficiency was calculated to be 38%. Such a phenomenon was ever attributed to side reactions with electrolyte and the formation of solid-electrolyte interface (SEI) film.[12] The efficiency went significantly up to 80% in the next cycle, then risen smoothly and reached 95% at the 10th cycle and 99% at the 30th. Note that the charge capacity was not uniformly increasing. It had a steady increase from 73 to 170 mAh g^{-1} in the first 20th cycles. Then the growth speed slowed down and the capacity is stabilized at about 180 mAh g^{-1} since the 30th cycle. The voltage profiles at the 30th and 40th cycles presented in Figure 4b are nearly totally overlapped, and differ greatly from that at the first cycle, though the discharge capacities are close.

The initial discharge curve can be roughly divided into three sections (Figure S2), which is quite similar to the case of anatase TiO_2 nanorods and nanoparticles[12, 25]. The voltage dropped to about 1.0 V rapidly with a delivered capacity less than 20 mAh g^{-1}, while in the second section the voltage change significantly slowed down in the range from 1.0 to 0.15 V, and most of the sodium ion uptake into the lattice happened here. This process would be enhanced in the subsequent cycles, as will be confirmed by the cyclic voltammetry test. The third section seems almost like a horizontal line, but not as long as in the reported work[12, 25]. It is presumed that the cubic anatase TiO_2 was not further reduced into metallic titanium, which will be proved below. After the initial cycle, the voltage profile
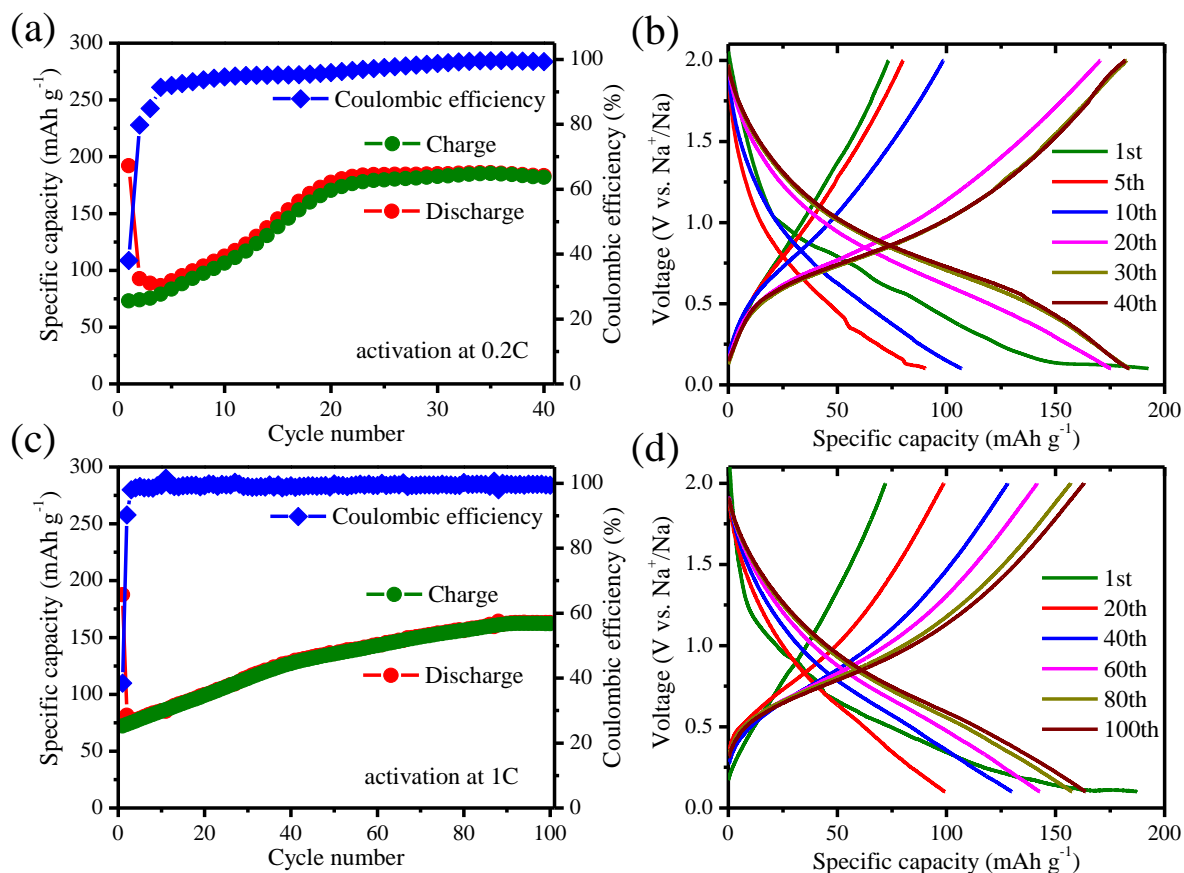
Figure 4. The specific capacities and coulombic efficiencies as well as the corresponding voltage profiles at selected cycles during the discharge/charge activation at 0.2C (a, b) and 1C (c, d). Note that 1C=168 mA g^{-1}.

could no longer be divided into three parts clearly, and the capacity went up slowly that is termed as activation in this paper.

The electrode was not fully activated until 30 discharge-charge loops ended at the rate of 0.2C. While in the case of 1C, the activation process took much more loops (nearly 90, Figure 4c). The charge capacity at the first, 20th, 40th, 60th, 80th and 100th is measured to be 72, 99, 128, 141, 156 and 162 mAh g^{-1} (Figure 4d). Despite the slower capacity growth, the coulombic efficiency is higher than at 0.2C. The initial one is 38.4%, and the second is already as high as 90.2%. It reached 99% at the 10th cycle and stabilized at this lever in the following cycles. After the activation of nearly 90 cycles, the cell hold a discharge and charge capacity of around 160 mAh g^{-1}. The first discharge voltage profile differs greatly form the 100th, just the same as at 0.2C. It can be interpreted that the recovered capacity during the activation process is not from the irreversible one in the initial discharge. The irreversibly inserted or converted sodium ions in initial cycles are always there, and the activation is plausibly to activate the inner part of nanocubes that have not yet functioned to play a role by repeated discharge-charge stimulations. A similar electrochemical activation phenomenon of Co_3O_4 hollow spheres as lithium-ion anodes was ever reported,[26] where the

capacity faded in the initial cycles and recovered in the subsequent cycles with no signs of further degradation.

This activation phenomenon is also reflected in the cyclic voltammetry (CV) curves, as shown in Figure 5. The measurement was conducted with a potential window of 2.0—0.1 V at a constant scan rate (0.2 mV s^{-1}) for 10 cycles. The first cathodic sweep started from the open circuit potential,
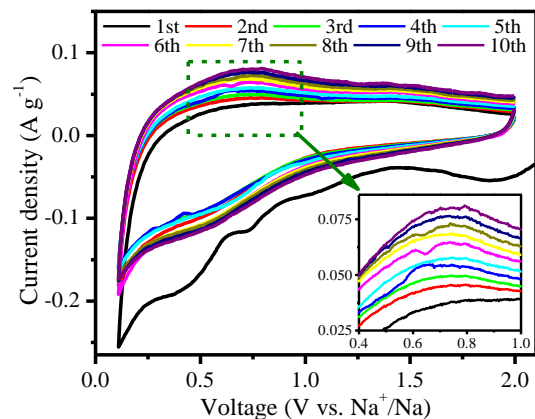
Figure 5. The cyclic voltammetry curves at the scan rate of 0.2 mV s^{-1} for the first ten cycles.
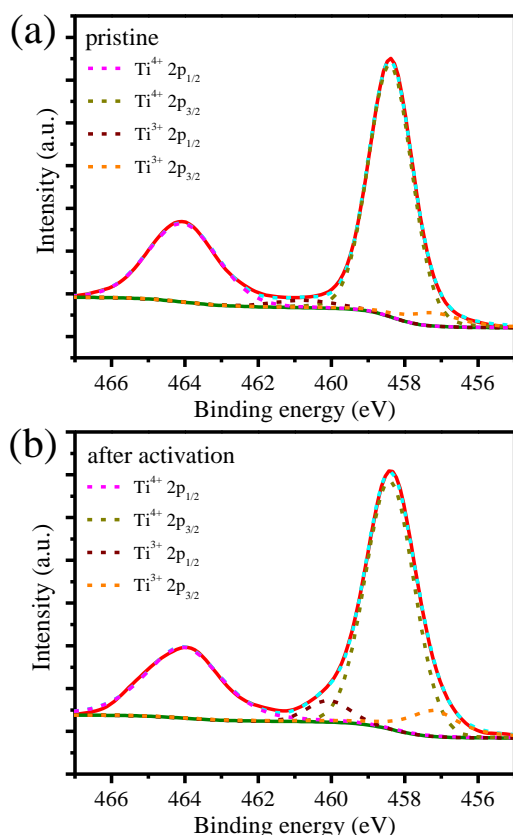
Figure 6. The Ti 2p spectrum of pristine (a) and activated electrodes.

about 2.3 V. The current density is far larger than that in the second cathodic sweep, which is consistent with the very big difference between the first two discharge capacities (Figure 4). Three seeming peaks are observed at around 1.8, 0.75 and 0.6 V, among them only the last one reappeared at following cathodic sweeps. Their origins are still not clear, and what's worse, they are so broad that each of them may correspond to several primitive processes. In anodic sweeps only one peak around 0.8 V is observed and reappeared in every anodic segment. It increased from 0.04 at the first loop up to 0.08 A g^{-1} at the 10th, as represented in the inset in Figure 5. The rising trend is in reasonable accordance with the galvanostatic discharge/charge activation.

In order to better understand the very low initial coulombic efficiency and the activation mechanism, we carried out an ex situ characterization with an X-ray photoelectron spectroscope (XPS). After total activation at 0.2C that ended up with a charge step, the coin cell was cracked open and the electrode film was fetched out (Figure S3) and dried in a vacuum oven at 80℃ before XPS characterization. The Ti 2p spectrum of both pristine and activated electrode films are given in Figure 6. There are two peaks at 463.9 and 458.4 eV ascribed to Ti^{4+} 2p$_{1/2}$ and Ti^{4+} 2p$_{3/2}$ in the spectra of the pristine electrode, which become obviously broader in that of the activated electrode. Undoubtedly, peaks for Ti species of lower valence state emerged irreversibly during the activation process. Both

the Ti 2p spectrum were deconvoluted before corrected by a Shirley-type background with two peak groups of Ti^{4+} 2p and Ti^{3+} 2p under the constraint that the ratio of 2p$_{1/2}$ and 2p$_{3/2}$ peak areas was fixed to be 1:2. The new peaks are ascribed to Ti^{3+} because the binding energy are located at 460.1 and 457.0 eV corresponding to Ti^{3+} 2p$_{1/2}$ and 2p$_{3/2}$. As presented in Figure 6a, there is a very low percentage of Ti^{3+} (about 7%) in the pristine electrode, which possibly originated from crystal defect like oxygen vacancies. In the activated electrode the percentage of Ti^{3+} increased up to about 13%, which means that an amount of sodium ions were irreversibly trapped into the lattice. Note that no formation of metallic Ti^{0} occurred that is quite different from the case of anatase TiO$_2$ nanoparticles[25]. Plausibly that's why the initial discharge capacity is much lower in this work.

2.3 Fast and durable performance

Rate capability and cycle stability were evaluated after a fully activation at 0.2C. The rate test was conducted in the range of 0.2—50C, 10 cycles at each rate (Figure 7). The specific capacity was respectively measured to be 180, 177, 174, 158, 132, 108, 84, 68, and 52 mAh g^{-1} at the rate of 0.2, 0.5, 1, 2, 5, 10, 20, 30, and 50C, (Figure S4) while the coulombic efficiency remained around 99%. As the rate increased, the potential polarization became severer and severer. At the rate of 50C (8.4 A g^{-1}), the recorded starting points of discharge and
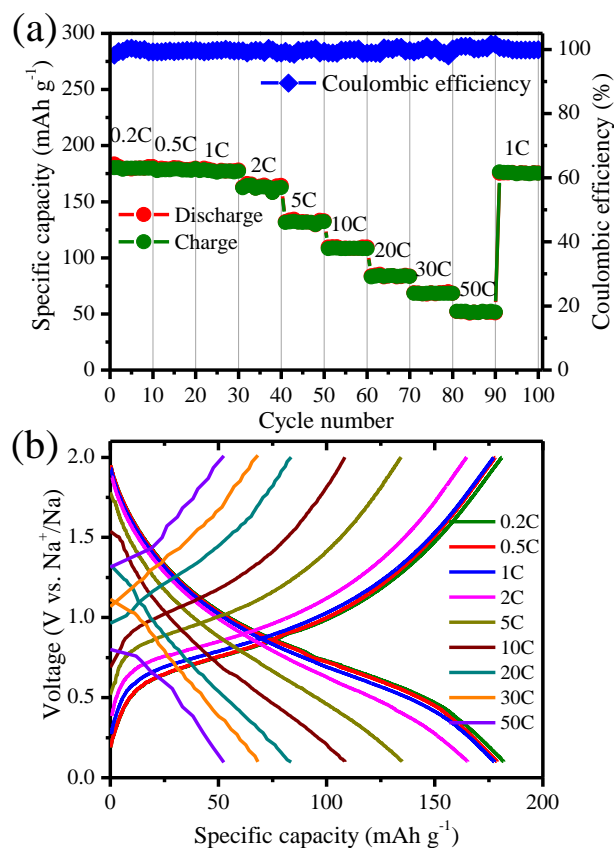
Figure 7. The specific capacity and coulombic efficiency (a) and discharge/charge voltage profiles (b) at various rates varying from 0.2C to 50C.
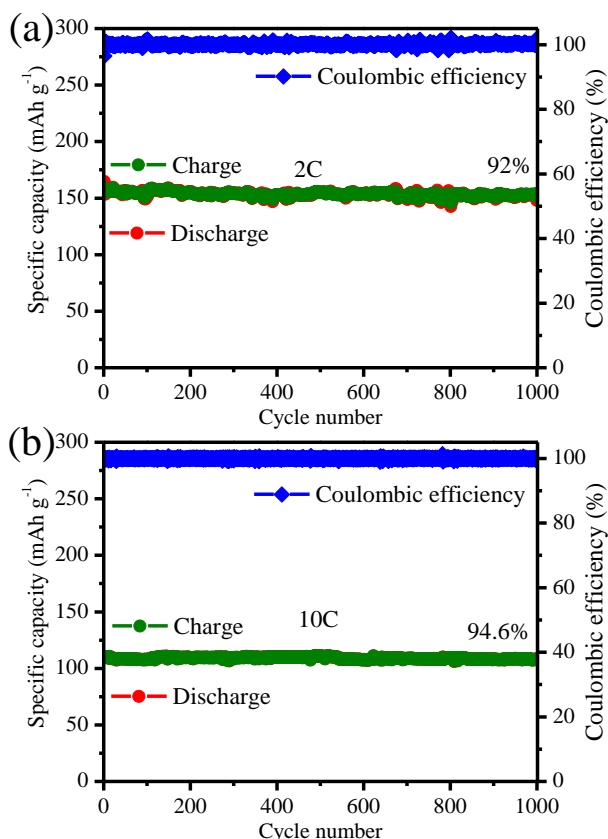
Figure 8. The specific capacity and coulombic efficiency for 1000 cycles at 2C (a) and 10C (b).

Figure 9. Three successive cyclic voltammetry curves at the constant scan rate of 0.2 mV s^{-1} (a) and at increasing scan rates from 0.2 mV s^{-1} to 5 mV s^{-1} (b).

charge voltage profile were 0.8 and 1.3 V, significantly away from the set value of 2.0 and 0.1 V (Figure 7b). Nevertheless, the capacity recovered to 173 mAh g^{-1} when the rate went back to 1C. The high-rate capacity is almost comparable to the performance of anatase TiO_2 nanorods coated with carbon[12] (the best ever reported).

The capability of enduring a fast sodiation and desodiation can make up for its relatively lower capacity than hard carbon[20] or tin and antimony alloy electrodes[21, 22], and shows a promising prospect for practical applications. Cycle stability was tested by 1000 loops of discharge and charge (Figure 8). At the rate of 2C, it delivered a specific capacity of about 153 mAh g^{-1} with a retention of 92%. The reversible specific capacity maintained 108 mAh g^{-1} at the rate of 10C with a higher retention of 94.6%. The voltage profiles at the first, 200th, 400th, 600th, 800th and 1000th cycles are provided in Figure S5 and S6 in the supplementary information. The amazing overlap indicates that not only was the capacity sustained, but also the specific discharge and charge procedures. In another words, there is almost no trace accumulation of discharge or charge that would take an effect on discharge or charge in the next cycle.

The performed cyclic voltammetry measurement with a constant scan rate of 0.2 mV s^{-1} confirmed the cell's stability, as displayed in Figure 9a. The voltammetry curves emerged from three successive sweeps are well overlapped. The voltammetry curves emerged from three successive sweeps are well overlapped. The weak anodic peak at 0.8 V in the fresh CV curves (Figure 5) had been seriously intensified after a long loop of discharge and charge. The cathodic peak at about 0.6 V was better shaped and much stronger than in Figure 5. It's reasonable to suppose that the electrochemical processes corresponding to the two redox peaks were the very ones activated in initial cycles. Along with the increasing scan rates (from 0.2 to 5 mV s^{-1}, Figure 9b), the anodic peak positively moved to 1.2 V that indicates a larger and larger polarization potential. The peak currents turned out to be linearly dependent on the square roots of scan rates, as presented in Figure S8. It means that the desodiation process is controlled by diffusion rather than a capacitive process, though the voltage profiles exhibited no well-defined discharge or charge plateaus. So the optimization of anatase TiO_2 electrode materials cannot be focused only on surface areas or porosity. Specially designed surface and bulk structures those can greatly facilitate the rate-determining diffusion are more direct factors. And they are not necessarily conflictive with factors like surface areas or porosity.

Heretofore, only a few reports have been done to the investigation of TiO_2 as NIB anodes. Their performances were organized in Table 1. Amorphous TiO_2 nanotubes grown on current collectors were employed in the pioneer work, and

Table 1. The comparison of reported works on anatase TiO_2 as NIB anodes.

Materials	Cut-off voltage (V)	Initial efficiency	Rate performance			Cycle stability	Ref
Nanotube [a]	2.5—0.5	~64%	70~150 mAh g^{-1} at 0.05 A g^{-1}			Gradually rising in the first 15 cycles	1
Nanocrystals	2.5—0.01	36.3%	mAh g^{-1}	150	~90[b]	~50[b]	Almost entirely stable up to 100 cycles at 0.05 A g^{-1}	9
			A g^{-1}	0.05	0.5	2		
Nanoparticles	2.0—0.1	52%	mAh g^{-1}	146	126	86	82% after 1000 cycles at 1.845 A g^{-1}	10
			A g^{-1}	0.037	0.369	3.69		
Nanorods	3.0—0.0	<30%	mAh g^{-1}	168	92	82	90.7% after 50 cycles at 1.65 A g^{-1}	12
			A g^{-1}	0.165	3.3	10		
Nanocubes	2.0—0.1	38.3%	mAh g^{-1}	176	132	84	94.6% after 1000 cycles at 1.68 A g^{-1}	This
			A g^{-1}	0.084	0.84	3.36		

Footnote: a) it is amorphous, not anatase type; b) the value is estimated from figures as not given in text.

delivered a gradually rising capacity at a very small rate (75~150 mAh g^{-1} at 50 mA g^{-1}).[1] The work using anatase TiO_2 nanocrystals intermixed with carbon demonstrated a stable sodium ion storage,[9] which benefitted from the contained carbon, but the capacity was to be sacrificed to some degree. Anatase TiO_2 nanoparticles, by contrast, revealed a much faster and more stable sodium ion uptake and release (150 mAh g^{-1} at 3.69 mA g^{-1}, 100 mAh g^{-1} at 185 mA g^{-1}, capacity retention of 82% after 1000 cycles at 185 mA g^{-1}).[10] A higher capacity and better rate performance were achieved by carbon-coated anatase TiO_2 nanorods, but cycle stability was not so good (168 mAh g^{-1} at 165 mA g^{-1}, 92 mAh g^{-1} at 3.3 A g^{-1}, nearly 10% loss within only 50 cycles at 1.65 A g^{-1}) that is presumably related with the cut-off potential.[12] To sum up the presented electrochemical data, anatase TiO_2 nanocubes used in this work behaved next to the best in terms of rate performance, and showed the best stability or reversibility if the activation process was put out of consideration.

2.4 Understanding of the superiority

The anatase TiO_2 nanocubes exhibited a superior performance in the comparison with nanotubes, nanoparticles, and so on. But how is the superiority brought about? The cycle stability can be supposed to be an inherent vantage of anatase TiO_2 according to its precedents.[10, 25] The repeatability of electrochemical behaviors is presumably put down to the recoverability of structure and morphology during sodiation/desodiation processes as perfectly confirmed by ex situ SEM and XRD characterization (Figure 10). The XRD pattern displayed that the sharp diffraction peaks remained at their original positions. Amazing! After thousands of sodium intake and release loops, the lattice structure is hardly changed. Some emerging peaks can be vaguely spotted at around 23 degree (2θ), which evidenced a small amount of residual sodium ions in the lattice in a certain extent. It is well consistent with previous XPS characterization. Based on the structure stability, the cubic morphology was expected to be

preserved. And the SEM images just turned out as expected: dispersed well-shaped nanocubes.

As for the rate capability, it cannot be simply attributed to the cubic shape. The exposing facets, the gateways of sodium ions from electrolyte into the lattice, inevitably influence the sodium ion uptake and release more or less. Whether it is a preferential facet is decided by the energy state of the crystal surface when sodium ion is attached. The energy change before and after sodium attachment is termed as attachment energy (E_{at}) here. It can be expressed as the following formula,

$$E_{at}=-(E_{Na-hkl}-E_{hkl}-E_{Na})/n \qquad \text{or}$$
$$E_{at}=-(E_{Na-hkl}-E_{hkl}-E_{Na})/2A$$

where E_{hkl} and E_{Na-hkl} are the total energy of surface-containing crystals before and after sodium atoms are attached on the {hkl} facets, E_{Na} is the total energy of sodium atoms, n is the number of attached sodium atoms, and A is the cross-sectional area. Herein we evaluated the attachment energy of sodium ions at different surfaces, namely, {100}, {001} and, {101} through first-principles calculations with the plane-wave pseudopotential method implemented in CASTEP package.[27] Before the calculation of E_{at}, we had checked the reliability of
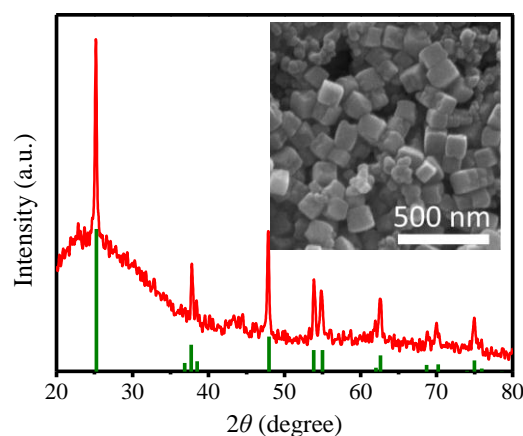
Figure 10. The ex situ XRD pattern and SEM image (inset).
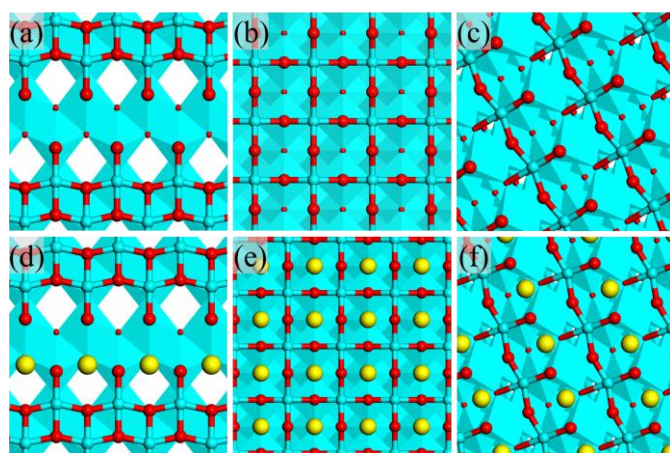
Figure 11. The clean {100}, {001} and {101} facets of anatase TiO_2 (a—c); the facets sodium atoms are attached on (d—f). The blue, red and yellow spheres are Ti, O and Na atoms.

the adopted method (Table S1 and S2).

The three kinds of surface were cleaved in a commonly used way and a vacuum slab of 15 Å was built to construct the surface-containing crystals (Figure 11a—11c). In order to build the model with sodium atoms attached, sodium atoms were inserted into the centre of oxygen octahedrons before surface cleaving and vacuum slab building, and then all sodium atoms except the ones on the surfaces were removed (Figure 11d—11e). The models in a pure ball-stick style were represented in the supplementary information (Figure S9 and S10).

The attachment energy was calculated to be 1.51, 0.33 and 0.50 eV (0.69, 0.37, and 0.41 J m^{-2}) for {100}, {001} and {101} facets respectively.[27-32] The {100} facets is distinctly much more energetically favorable than {001} and {101} in terms of whether per unit sodium atom or per unit surface area. This may result from the monatomic steps on the {100} facets where sodium atoms can be better accommodated. The obtained anatase TiO_2 nanocubes were encircled by four {100} facets, just like a belt. Such surface structures endowed the nanocubes with higher reactivity, thus enabled them to undertake a rapid uptake and release of sodium ions.

The relevance of surface structure to electrochemical behaviour in the case of $LiFePO_4$ was investigated via simulation techniques.[33] Except the attachment energy, the most facile direction of lithium ion diffusion was also supposed to have an influence. Coincidently and thankfully, the zigzag tunnels of open-structured anatase TiO_2, along which charge carriers would be transported most probably, are normal to the {100} facets with the lowest attachment energy (Figure 11a). In a nutshell, sodium ions are most facile to be attached to the four {100} facets encircling the nanocubes, and most convenient to be transport along [100] directions. So when seen from this perspective the superiority of sodium ion battery performance is no surprising.

Conclusions

This is the first work that employing anatase TiO_2 nanocubes as NIB anodes. An activation process was observed before the nanocubes could deliver a stable capacity. During the activation it is the electrochemical process corresponding to the cathodic voltage of ~0.6 V or the anodic voltage of ~0.8 V that was enhanced. The final reversible capacity is comparable to ever published work though the initial discharge capacity is small. The analysis of Ti 2p species based on ex situ XPS characterization of both pristine and activated electrode indicates that a number of sodium ions were trapped in the lattice, but no metallic Ti^0 was produced. It partially accounts for the low initial discharge and irreversible capacity. In the consideration of limited sodium source from cathodes, the nanocubes are obviously more advantageous than nanoparticles or nanorods[10, 12]. In the subsequent discharge-charge tests, excellent rate performance and outstanding cycle stability were presented. When the galvanostatic current increased from 0.2C to 10C, the specific capacity varied from 180 to 108 mAh g^{-1} with a retention of 60%. Within the 1000 cycles at the rate of 2C and 10C, the capacity loss is less than 10%, which is extraordinary in the existing literature. The superior performance is related to the exposed {100} facets surrounding the nanocubes, as they are favorable for sodium attachment according to our first-principles calculations and the most possible diffusion directions are normal to {100} facets.

The study on the surface or interface of electrode materials is of common significance for the optimization of battery performance, but the effect of exposing crystal facets, extensively explored in catalysis[34, 35], is rarely emphasized in LIB or NIB electrodes. The status is caused, to our point of view, mainly from the scarce of controllable synthesis of single crystals and the complexity of comprehension more than the effect of structure architectures such as hollow spheres, nanotubes, nanosheets and so on. Besides, experimental comparison of different facets with the influence of sizes excluded is also a big challenge so far. Fortunately, we can make it by resorting to theoretic methods. The calculated results here supported the superior performance of as-prepared nanocubes, and it can be easily deduced that tetragonal nanofibers, of which the length in [100] or [010] direction is much smaller, shall have a better NIB performance.

Notes and references

[a] College of Chemistry and Chemical Engineering, Central South University, Changsha 410083, China.

[b] School of Energy Science and Engineering, University of Electronic Science and Technology of China, Chengdu, 611731, China

1. H. Xiong, M. D. Slater, M. Balasubramanian, C. S. Johnson and T. Rajh, *J Phys Chem Lett*, 2011, **2**, 2560-2565.

2. J. B. Goodenough and Y. Kim, *J Power Sources*, 2011, **196**, 6688-6694.

3. J. B. Goodenough and K.-S. Park, *J Am Chem Soc*, 2013, **135**, 1167-1176.

4. D. L. Wood Iii, J. Li and C. Daniel, *J Power Sources*, 2015, **275**, 234-242.

5. M. D. Slater, D. Kim, E. Lee and C. S. Johnson, *Adv Funct Mater*, 2013, **23**, 947-958.

6. S. P. Ong, V. L. Chevrier, G. Hautier, A. Jain, C. Moore, S. Kim, X. Ma and G. Ceder, *Energy Environ Sci*, 2011, **4**, 3680-3688.

7. S.-W. Kim, D.-H. Seo, X. Ma, G. Ceder and K. Kang, *Adv Energy Mater*, 2012, **2**, 710-721.

8. P. Barpanda, G. Oyama, S.-i. Nishimura, S.-C. Chung and A. Yamada, *Nat Commun*, 2014, **5**.

9. Y. Xu, E. Memarzadeh Lotfabad, H. Wang, B. Farbod, Z. Xu, A. Kohandehghan and D. Mitlin, *Chem Commun*, 2013, **49**, 8973-8975.

10. L. Wu, D. Buchholz, D. Bresser, L. Gomes Chagas and S. Passerini, *J Power Sources*, 2014, **251**, 379-385.

11. K. Kuratani, N. Uemura, H. Senoh, H. T. Takeshita and T. Kiyobayashi, *J Power Sources*, 2013, **223**, 175-182.

12. K.-T. Kim, G. Ali, K. Y. Chung, C. S. Yoon, H. Yashiro, Y.-K. Sun, J. Lu, K. Amine and S.-T. Myung, *Nano Lett*, 2014, **14**, 416-422.

13. M. Okoshi, Y. Yamada, A. Yamada and H. Nakai, *J Electrochem Soc*, 2013, **160**, A2160-A2165.

14. N. Yabuuchi, K. Kubota, M. Dahbi and S. Komaba, *Chem Rev*, 2014, **114**, 11636-11682.

15. P. Senguttuvan, G. Rousse, V. Seznec, J.-M. Tarascon and M. R. Palac ń, *Chem Mater*, 2011, **23**, 4109-4111.

16. Z. Bi, M. P. Paranthaman, P. A. Menchhofer, R. R. Dehoff, C. A. Bridges, M. Chi, B. Guo, X.-G. Sun and S. Dai, *J Power Sources*, 2013, **222**, 461-466.

17. A. Rudola, K. Saravanan, C. W. Mason and P. Balaya, *J Mater Chem A*, 2013, **1**, 2653-2662.

18. Y. Yang, B. Qiao, X. Yang, L. Fang, C. Pan, W. Song, H. Hou and X. Ji, *Adv Funct Mater*, 2014, **24**, 4349-4356.

19. G. A. Seisenbaeva, J.-M. Nedelec, G. Daniel, C. Tiseanu, V. Parvulescu, V. G. Pol, L. Abrego and V. G. Kessler, *Chem Eur J*, 2013, **19**, 17439-17444.

20. S. Komaba, W. Murata, T. Ishikawa, N. Yabuuchi, T. Ozeki, T. Nakayama, A. Ogata, K. Gotoh and K. Fujiwara, *Adv Funct Mater*, 2011, **21**, 3859-3867.

21. L. D. Ellis, T. D. Hatchard and M. N. Obrovac, *J Electrochem Soc*, 2012, **159**, A1801-A1805.

22. H. Hou, M. Jing, Y. Yang, Y. Zhu, L. Fang, W. Song, C. Pan, X. Yang and X. Ji, *ACS Appl Mater Inter*, 2014, **6**, 16189-16196.

23. X. Zhao, W. Jin, J. Cai, J. Ye, Z. Li, Y. Ma, J. Xie and L. Qi, *Adv Funct Mater*, 2011, **21**, 3554-3563.

24. X. Yang, Y. Yang, H. Hou, Y. Zhang, L. Fang, J. Chen and X. Ji, *J. Phys. Chem. C*, 2015, **119**, 3923-3930.

25. L. Wu, D. Bresser, D. Buchholz, G. Giffin, C. R. Castro, A. Ochel and S. Passerini, *Adv Energy Mater*, 2015, **5**, n/a-n/a.

26. H. Sun, G. Xin, T. Hu, M. Yu, D. Shao, X. Sun and J. Lian, *Nat Commun*, 2014, **5**, 5526.

27. S. J. Clark, M. D. Segall, C. J. Pickard, P. J. Hasnip, M. I. Probert, K. Refson and M. C. Payne, *Zeitschrift für Kristallographie*, 2005, **220**, 567-570.

28. J. Neugebauer and M. Scheffler, *Phys Rev B*, 1992, **46**, 16067.

29. J. Andzelm, R. King-Smith and G. Fitzgerald, *Chem Phys Lett*, 2001, **335**, 321-326.

30. M. C. Payne, M. P. Teter, D. C. Allan, T. Arias and J. Joannopoulos, *Rev Mod Phys*, 1992, **64**, 1045.

31. W. Kohn and L. J. Sham, *Phys Rev*, 1965, **140**, A1133.

32. P. Hohenberg and W. Kohn, *Phys Rev*, 1964, **136**, B864.

33. C. A. Fisher and M. S. Islam, *J Mater Chem*, 2008, **18**, 1209-1215.

34. S. Liu, J. Yu and M. Jaroniec, *J Am Chem Soc*, 2010, **132**, 11914-11916.

35. J. Pan, G. Liu, G. Q. M. Lu and H. M. Cheng, *Angew Chem Int Ed*, 2011, **50**, 2133-2137.
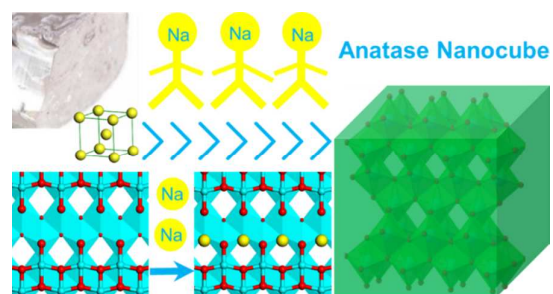
Anatase TiO_2 nanocubes were employed as sodium ion battery anodes and delivered an outstanding rate and cycle performance after an interesting activation process.